Neurobiology of Disease 153 (2021) 105317

Contents lists available at ScienceDirect

Neurobiology of Disease

journal homepage: www.elsevier.com/locate/ynbdi

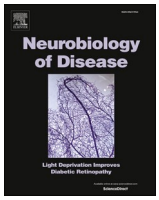

SGK1.1 limits brain damage after status epilepticus through M current-dependent and independent mechanisms

Elva Martin-Batista [a,b], Laura E. Maglio [a,b], Natalia Armas-Capote [a,b], Guadalberto Hernández [a,b], Diego Alvarez de la Rosa [a,b], Teresa Giraldez [a,b,*]

[a] Departamento de Ciencias Médicas Básicas, Facultad de Medicina, Universidad de La Laguna, Campus de Ciencias de la Salud sn, 38200 San Cristobal de La Laguna, Spain

[b] Instituto de Tecnologías Biomédicas (ITB), Campus de Ciencias de la Salud sn, 38071 San Cristobal de La Laguna, Spain

ARTICLE INFO

Keywords:
Serum and glucocorticoid-regulated kinase 1
KA-induced seizures
Neuroprotection
Epilepsy
Kv7 potassium channels
Apoptosis

ABSTRACT

Epilepsy is a neurological condition associated to significant brain damage produced by status epilepticus (SE) including neurodegeneration, gliosis and ectopic neurogenesis. Reduction of these processes constitutes a useful strategy to improve recovery and ameliorate negative outcomes after an initial insult. SGK1.1, the neuronal isoform of the serum and glucocorticoids-regulated kinase 1 (SGK1), has been shown to increase M-current density in neurons, leading to reduced excitability and protection against seizures. For this study, we used 4–5 months old male transgenic C57BL/6 J and FVB/NJ mice expressing near physiological levels of a constitutively active form of the kinase controlled by its endogenous promoter. Here we show that SGK1.1 activation potently reduces levels of neuronal death (assessed using Fluoro-Jade C staining) and reactive glial activation (reported by GFAP and Iba-1 markers) in limbic regions and cortex, 72 h after SE induced by kainate, even in the context of high seizure activity. This neuroprotective effect is not exclusively through M-current activation but is also directly linked to decreased apoptosis levels assessed by TUNEL assays and quantification of Bim and Bcl-x_L by western blot of hippocampal protein extracts. Our results demonstrate that this newly described antiapoptotic role of SGK1.1 activation acts synergistically with the regulation of cellular excitability, resulting in a significant reduction of SE-induced brain damage in areas relevant to epileptogenesis.

1. Introduction

Epilepsy is a neurological disease characterized by recurrent and unpredictable seizures, affecting more than 50 million people around the world. Temporal Lobe Epilepsy (TLE) is one of the most common types of epilepsy and the most refractory to treatment in humans. Two-thirds of TLE patients develop a sclerosis state caused by neuronal loss and gliosis (Mathern et al., 1997). Epileptogenesis has been associated to neurodegeneration, gliosis, uncontrolled inflammation, and aberrant neurogenesis. These alterations in brain homeostasis often results in a chronic epileptic condition (Pitkanen and Lukasiuk, 2009b). Therefore, there is an increasing interest in the field of epilepsy research to develop new therapies targeting neuronal death and inflammation pathways.

According to the International League Against Epilepsy (ILAE), status epilepticus (SE) is defined as a period of continuous behavioral or electroencephalographic seizures resulting either from the failure of the mechanisms responsible for seizure termination or from the initiation of mechanisms which lead to abnormally prolonged seizures (Trinka et al., 2015). Chemically-induced-SE animal models reproduce most behavioral, electroencephalographic and neuropathological characteristics of TLE and have been widely used in basic epilepsy research to study this disorder (Levesque et al., 2016). SE-triggered negative outcomes in the brain include neuronal death, which has been associated to the appearance of new seizures. Over-activation of glutamate receptors following SE constitutes a major cause of neuronal death. Elevation of Na^+ and Ca^{2+} influx eventually leads to membrane disruption, cell lysis, release of free radicals and DNA degradation (Pitkanen and Lukasiuk, 2009a). In addition, alterations in the expression of various biochemical markers for apoptosis have been related to seizure-induced neuronal loss, including members of the Bcl-2 gene family and caspases (Kim

* Corresponding author at: Departamento de Ciencias Médicas Básicas, Facultad de Medicina, Universidad de La Laguna, Campus de Ciencias de la Salud sn, 38200-San Cristobal de La Laguna, Spain

E-mail addresses: emartinb@ull.edu.es (E. Martin-Batista), lamaglio@ull.edu.es (L.E. Maglio), narmasca@ull.edu.es (N. Armas-Capote), ghernan@ull.edu.es (G. Hernández), dalrosa@ull.edu.es (D. Alvarez de la Rosa), giraldez@ull.edu.es (T. Giraldez).

https://doi.org/10.1016/j.nbd.2021.105317
Received 6 October 2020; Received in revised form 4 February 2021; Accepted 22 February 2021
Available online 24 February 2021

et al., 2014). Therefore, neuroprotection could be facilitated by two different but not necessarily unrelated general mechanisms. First, the activation of pathways limiting excitability. Secondly, the prevention of downstream events leading to apoptosis.

We have recently shown that increased activity of SGK1.1, the neuronal isoform of the serum and glucocorticoids-regulated kinase 1 (SGK1) potently reduces seizure duration and severity in a kainic acid (KA)-induced SE paradigm with transgenic mice expressing a permanently active form of the kinase (Armas-Capote et al., 2020). Electrophysiological measurements in sympathetic neurons (Miranda et al., 2013) and hippocampal brain slices (Armas-Capote et al., 2020) showed that SGK1.1 up-regulates the neuronal M- current mediated by Kv7.2/7.3 ion channels. Altogether, our data suggested that SGK1.1 activation may provide a mechanism securing the brain against epilepsy-related neuronal damage by controlling neuronal excitability. However, our previous studies did not include evaluation of neuronal death or any process associated to neurodegeneration.

In addition to the control of neuronal excitability, different studies have demonstrated that seizure-induced neuronal loss can be diminished by molecular and pharmacological approaches limiting apoptotic cell death (Henshall et al., 2002; Roy et al., 2002). Interestingly, SGK1 isoforms share high homology to the catalytic domain of the well described anti-apoptotic kinase AKT (Kobayashi et al., 1999). Both AKT and its upstream activator PI3K have been demonstrated to reduce apoptosis and promote neuronal survival in the central nervous system (Crowder and Freeman, 1998; Datta et al., 1997). The ubiquitous isoform SGK1 shows cell-survival and anti-apoptotic effects (Brunet et al., 2001; Ferrelli et al., 2015) and has been linked to neuroprotection in stroke (McCaig et al., 2019; Wang et al., 2019). Taking all this into account, we hypothesized that in addition to the observed reduction in neuronal excitability, SGK1.1 activation could directly reduce apoptosis levels post-SE and that the combination of both processes may act synergistically to limit neuronal death and brain damage. In this study we show that transgenic expression of constitutively active SGK1.1 dramatically reduces neuronal death and subsequent inflammatory processes associated to KA-induced seizures. This effect was only partially prevented by M-current inhibition and is associated to altered levels of apoptotic biomarkers consistent with lower apoptosis levels. In summary, we demonstrate the existence of a dual mechanism underlying SGK1.1-mediated protection against neuronal death involving not only the modulation of neuronal excitability, but also the additional modulation of cellular pathways leading to apoptosis.

2. Material and methods

2.1. Animals and seizure induction

Animal handling and experimental procedures were approved by Universidad de La Laguna Ethics Committee and conform to Spanish and European guidelines for protection of experimental animals (RD53/2013; 2010/63/EU). Animals were housed in groups of 3–4 per cage, in conditions of constant temperature (21–22 °C), a 12 h light/dark cycle, and given free access to standard chow and water. Effort was made to minimize animal suffering and number. This work is based on the use of a transgenic mouse model previously generated in our laboratory, B6.Tg.sgk1 (Armas-Capote et al., 2020; Miranda et al., 2013). Briefly, the mouse model was created using bacterial artificial chromosome (BAC)-mediated transgenesis, a well-established methodology (Yang and Gong, 2005). In our case, the BAC, obtained from BACPAC Resources Center (Children's Hospital Oakland Research Institute, Oakland, CA, USA), included 180 kbp of the mouse genome containing the whole *Sgk1* gene and its regulatory elements. The BAC transgene expresses *Sgk1* splice isoforms under their own promoters, results in near physiological expression levels of the neuronal isoform SGK1.1 in the brain, avoiding deleterious effects of kinase over expression (Armas-Capote et al., 2020; Arteaga et al., 2008; Miranda et al., 2013). In addition, the Sgk1 transgene included a point mutation (S422D in the ubiquitous isoform SGK1; S515D in the neuronal isoform SGK1.1) that renders the kinase constitutively active (Kobayashi and Cohen, 1999). As a consequence, the expression levels of SGK1.1 were nearly physiological, but the kinase activity in the transgenic mice was significantly increased (Armas-Capote, 2017). Founder animals were backcrossed with wild type C57BL/6 J for at least nine generations. All experiments described here were performed in homozygous mice obtained by crossing heterozygous animals. FVB.Tg.sgk1 mice were generated by transferring the transgene to the inbred strain FVB/N, backcrossing for 9 generations (Armas-Capote et al., 2020). Wild-type mice (B6.WT or FVB.WT) in the same genetic background (C57BL/6 J or FVB/N) were used as controls. Seizures were induced in 16–22 weeks-old mice with intraperitoneal (ip) injection of 20 mg/kg KA (K0250; Sigma Aldrich) as previously described (Armas-Capote et al., 2020). Seizure behavior was evaluated in male mice for 2 h post-KA injection using a modified Racine scale: 0, no response, 1, immobility, 2, rigid posture and tail extension, 3, head bobbing and repetitive movements, 4, rearing, 5 rearing and falling continuously, 6, tonic-clonic generalized seizures and 7, death. This time frame for seizure behavior experiments was estimated as optimal based in the existing literature and previous work by our group (Armas-Capote et al., 2020; Miranda et al., 2013). In brief, we quantified the duration of SE (Stages 1–6) in our experimental model as the time elapsed from the administration of chemoconvulsant and the end of behavioral seizures, as described previously (*e.g.*Ben-Ari et al., 1979; Klement et al., 2018; Takahashi et al., 2010; for reviews, see also Sharma et al., 2007; Sharma et al., 2018). Only male mice surviving after reaching score 6 were included in the histological studies. Where indicated, 10 mg/kg XE991 (X2254, Sigma Aldrich) or 1.6 mg/kg EMD638683 (HY-15193A, MedChem Express) were administered ip 1 h or 1 day prior to KA injection respectively, as described elsewhere (Armas-Capote et al., 2020). EMD638683 is a highly selective SGK1 inhibitor, which counteracts the activity and physiological effects of SGK1 with an IC50 of 3 μM (Ackermann et al., 2011). XE991 is a potent analogue of linopirdine, blocking the KCNQ2/3 heteromeric M current with an IC50 of 2.5 μM (Zaczek et al., 1998). Mice injected with saline were used as controls.

2.2. Sample preparation and image acquisition

A selection of male mice reaching Racine stage 6 (generalized tonic-clonic seizures) was used for analysis of neurodegeneration and gliosis (see corresponding sections below). The time frame for sample preparation (72 h after KA injection) was determined as the moment for optimal detection of the parameters studied (neuronal death by FJC-labelling, astrogliosis and microgliosis), based on preliminary experiments performed in our laboratory (data not shown) and the existent literature (*e.g.* Benkovic et al., 2004; Kim et al., 2014; Zanuzzi et al., 2019). The number of animals used for each experiment is specified in the corresponding figure legends. Male mice were deeply anesthetized with an overdose of sodium pentobarbital and transcardially perfused with heparinized ice-cold 0,9% saline followed by paraformaldehyde (PFA) 4% in 0.1 M phosphate-buffered saline pH 7.4 (PBS). The brains were removed and stored overnight in the same fixative at 4 °C, cryoprotected in 30% (w/v) sucrose-PBS solution and stored at −80 °C until processing. Coronal sections (30 μm) were obtained with a freezing microtome (Thermo Fisher), collected in 5–7 parallel series and processed for FJC or immunofluorescence (see below for details about each procedure). Individual sections were examined using confocal microscopy (Leica TCS SP8). All microscopic and computer parameters were maintained constant throughout each study (FJC, astrogliosis or microgliosis quantification). Imaging included the following brain areas: hippocampus, piriform cortex, entorhinal cortex, somatosensorial cortex, auditive cortex, and amygdala, using the Franklin and Paxinos mouse atlas (Franklin and Paxinos, 2008) as a guide (Supplementary Fig. 1). Image analysis was performed using ImageJ-Fiji software (Schindelin et al., 2012). Specific details about image analysis

procedures used in each experiment are provided in the sections below. For western blot experiments, hippocampi were collected 24 h after KA treatment as previously described (Kim et al., 2014). Protein extracts were obtained by processing samples with lysis buffer (Tris-Base 0.5 M, pH 7.4; SDS 10%) containing phosphatase and proteinase inhibitors (Roche). Lysates were clarified by centrifugation at 14000 xg for 10 min and protein concentration was measured using the bicinchoninic acid assay.

2.3. Neurodegeneration quantification by Fluoro-Jade C staining

Neuronal degeneration was detected using Fluoro-Jade C (FJC; AG325, Millipore), an anionic fluorochrome capable of selectively staining degenerating neurons in brain slices (Schmued et al., 2005), following a previously described protocol (Afonso-Oramas et al., 2010). Image analysis: 1) FJC-positive (FJC+) cells were identified as green fluorescent cells over the background fluorescence threshold. 2) The same threshold value was used for all measurements. 3) Number of FJC+ cells was quantified using the "analyze particles" function in Fiji (Schindelin et al., 2012) and normalized to the area of the region studied. 4) FJC+/area values were averaged to obtain one final measurement per brain region. Cell counts were conducted in five sections 245 μm away from each other and five microscopic fields per section were selected by an independent observer blinded to gliosis and seizure behavior data.

2.4. Gliosis quantification by immunohistochemistry

The presence of reactive gliosis was assessed by measuring the expression of glial fibrillary acidic protein (GFAP) in astrocytes (astrogliosis) and ionized calcium-binding adapter molecule 1 (Iba-1) in microglia (microgliosis). Briefly, sections were washed three times with PBS, blocked with 4% goat serum for 1 h and incubated overnight with anti-GFAP antibodies (G3893, Sigma-Aldrich) at 1:400 or anti-Iba-1 antibodies (ab5076, Abcam) at 1:500 diluted in 2% goat serum. Sections were then washed 3–4 times in PBS before incubation with secondary antibodies conjugated to Alexa Fluor® 594 (A-11005, Thermo Fisher Scientific) at 1:200 or Alexa Fluor® 488 (ab150141, Abcam) at 1:1000 for 2 h. Finally, sections were washed and mounted with Mowiol and 4′,6-diamidino-2-phenylindole (DAPI). Image analysis: 1) blue (DAPI) and red (GFAP, astrogliosis) or green (Iba1, microgliosis) channels were quantified separately. 2) For each channel, we quantified the area occupied by fluorescent signals over the background threshold after noise elimination using standard Fiji procedures. 3) For each image, the corresponding ratios 'GFAP area/DAPI area' and 'Iba1 area/DAPI area' were calculated. 4) In order to compare the extent of SGK1.1 activation on astrogliosis and microgliosis in the different brain regions, fluorescent area ratios corresponding to WT were assigned a 100% value to which transgenic mice data were normalized. One section (between −1.755 and − 2.155 mm from Bregma) was selected for cell counts conducted in five microscopic fields per section by an independent observer blinded to FJC and seizure behavior data.

2.5. SGK1.1 cellular localization by immunohistochemistry

A rabbit polyclonal antibody against SGK1.1 was generated against a glutathione S-transferase (GST) fusion protein containing amino acids 41–80 from the SGK1.1-specific exon 2, expressed in E. coli and purified by affinity chromatography. Using glutathione-agarose beads in a column elution system (Frangioni and Neel, 1993). Eluates were analyzed by electrophoresis in stain free 10% polyacrylamide gels. Immunization was performed using aliquots of 0.5 mL mixed with 0.5 mL of Freud adjuvant. SGK1.1 expression in brain slices (obtained as described above) was assessed by immunohistochemistry (see above), using this newly-generated polyclonal anti-SGK1.1 antibody at a final concentration ranging 1:100–1:500 followed by secondary antibody anti-rabbit Alexa Fluor® 488 (A-11008, Thermo Fisher Scientific) at 1:500. Co-staining of sections was performed with one of the following markers: Calcium-calmodulin-dependent protein kinase II (CAMKII), detected with a specific anti-CAMKII (1:400; MA1–048, Abcam); parvalbumin (PV), detected with anti-PV antibodies (1:300; P3088, Santa Cruz Biotechnology); GFAP, detected using anti-GFAP (G3893, Sigma Aldrich). Detection of markers used secondary anti-mouse Alexa Fluor® 594 (1:200; A-11005, Thermo Fisher Scientific).

2.6. Western blot analysis

Proteins were separated by SDS denaturing gel electrophoresis (SDS-PAGE), transferred to a polyvinylidene fluoride membrane and analyzed by western blot (WB). In order to gain a further insight into the anti-apoptotic role of SGK1.1, we measured the levels of two apoptotic factors. Antibodies against Bcl-2 interacting mediator of cell death (Bim) and B-cell lymphoma-extra-large (Bcl-x_L) were obtained from Santa Cruz Biotechnology (Santa Cruz, CA; sc-374,358 and sc-8392, respectively). Chemiluminescence signals were quantified using Image Lab® software 6.0 (Bio-Rad). Total protein fluorescence staining (stain-free™, BioRad) was used as loading control.

2.7. Cell culture and transfection

Human embryonic kidney cells HEK293T were obtained from the American Type Culture Collection (Manassas, VA) and maintained in DMEM supplemented with 10% FBS. Cells were transfected 24–48 h before experiments using Jetprime (Polyplus Transfection) following the manufacturer's instructions. Plasmid constructs for WT or mutant SGK1.1 have been previously described (Arteaga et al., 2008; Wesch et al., 2010). Construct AKT-myr expressing a constitutively active form of AKT fused to a myristoylation signal sequence was was a gift from William Sellers (obtained from Addgene, plasmid # 9009 (Ramaswamy et al., 1999)). pECFP-N1 was obtained from Clontech.

2.8. SGK1.1 immunostaining in cell cultures

We performed immunochemistry assays on HEK293T cells transiently transfected with pECFP-N1 (used as negative control) or pECFP-SGK1.1-N1, using the primary antibody generated in this study (see above). Transfected cells were identified as CFP-blue fluorescent cells. SGK1.1 expression was detected by standard immunostaining protocols (Coric et al., 2004) using our novel polyclonal antibody at 1:5000 and anti-rabbit Alexa Fluor® 594 (A-11042, Thermo Fisher Scientific) at 1:200.

2.9. Terminal deoxynucleotidyl transferase dUTP nick end labeling (TUNEL) assay

In order to evaluate the potential anti-apoptotic role of SGK1.1 and compare it to AKT's, we performed TUNEL assays in HEK293T cells. Briefly, cells were transiently transfected with SGK1.1 dominant negative mutant (SGK1.1^{K220A}), a mutant rendering the kinase constitutively active (SGK1.1^{S515D}) or a mutant targeting it to the nucleus (SGK1.1^{FF19,20AA}). AKT was used as a positive control for anti-apoptotic effects. An empty vector (pECFP-N1) was used to control for transfection toxicity. Cells were treated with 1 mM hydrogen peroxide (H_2O_2) for 4 h to induce apoptosis. The TUNEL protocol was performed using a commercial kit (ApopTag® fluorescein *in situ* apoptosis detection kit, Millipore) and following the manufacturer protocol. Coverslips containing the different cell preparations were examined using confocal microscopy (Leica TCS SP8) and analyzed using ImageJ-Fiji software. All images were obtained using the same microscope settings. Five replicates of each condition were imaged and analyzed. Quantifications were performed on at least 6 different fields per condition replicate, which were then averaged. Briefly, number of TUNEL-positive cells was obtained by

quantifying green-fluorescent cells corresponding to fluorescein-labelling of single- and double-stranded DNA breaks associated with apoptosis. The total proportion of TUNEL-positive cells for each condition was obtained by dividing the TUNEL-positive cells number by the total number of cells counted in the DAPI fluorescence channel. Finally, comparison of all conditions tested was done by assigning a 100% value to cells transfected with the pECFP-N1 control, to which all other data were normalized. These final calculations correspond to the data shown in Fig. 6B.

2.10. Experimental design and statistical analysis

Statistical analysis was performed using Prism 8 (GraphPad). Prior to any statistical analysis, we assessed normality distribution of our data using D'Agostino-Pearson or Shapiro-Wilk normality test. Once normality was established, we compared data means using t-test for comparisons of two groups or one-way ANOVA test for more than two groups for parametric distributions and Mann-Whitney for non-parametric distributions. Specific statistical tests and number of animals are indicated in each figure legend. It is important to note that to ensure objectivity in the imaging quantification process, each test sample was measured under the same experimental conditions by two different observers.

3. Results

3.1. SGK1.1 protects mice from kainate-induced neuronal death

We have previously shown that transgenic mice expressing a constitutively active form of the kinase (B6.Tg.sgk1) show significantly reduced seizure severity in the KA-induced SE animal paradigm (Armas-Capote et al., 2020). This is reflected in fewer mice reaching more severe Racine stages and associated mortality (Fig. 1A). In this study we evaluated the impact of increased SGK1.1 activity in neurodegeneration and gliosis on mice surviving acute seizures after KA treatment. For this purpose, we selected mice reaching Racine stage 6 (generalized tonic-clonic seizures; Fig. 1A, orange box). We reasoned that the comparison of transgenic mice with their WT counterparts that are reaching comparable seizure severity levels would allow us to unveil the potential contribution of additional neuroprotective mechanisms activated by SGK1.1 independent of seizure protection (Armas-Capote et al., 2020). Neurodegeneration was quantified by FJC staining of brain slices from B6.WT and B6.Tg.sgk1 mice reaching tonic-clonic seizures (Racine 6). As shown in Fig. 1B (left panels), significant levels of neuronal damage were observed in B6.WT mice, reflected as a significant number of FJC-stained cells (Fig. 1C). This result was comparable to previous reports using similar experimental conditions (Hopkins et al., 2000; Yan et al., 2018). In contrast, activation of SGK1.1 in B6.Tg.sgk1 neurons conferred a remarkable level of protection against neuronal death in all brain areas studied, including hippocampus, somatosensorial auditive and piriform-entorhinal cortex (Fig. 1B, right panels, and Fig. 1C). This observation is especially striking taking into account that all analyzed samples were obtained from B6.Tg.sgk1 mice reaching tonic-clonic convulsions, suggesting the possibility that protective mechanisms are activated by SGK1.1 even in conditions of neuronal hyperexcitability. The neuroprotective effect associated to SGK1.1 activation was not specific of the C57BL/6 J genetic background. Similar results were obtained with transgenic mice generated on the FVB background, which has been proposed to display increased seizure susceptibility to KA (Loscher et al., 2017) (Fig. 1D–F).

To ensure that the observed effects were a direct consequence of kinase activity, mice were acutely pre-treated with the SGK1.1 inhibitor EMD638683. As shown in Fig. 2A and consistent with our previous report (Armas-Capote et al., 2020), inhibition of the kinase reverted the protective effect and abolished all differences in seizure behavior between genotypes (Fig. 2A). These animals showed indeed higher levels of mortality (Fig. 2A, blue trace). A direct consequence of this effect is that the WT + EMD mice that we were able to select for the study

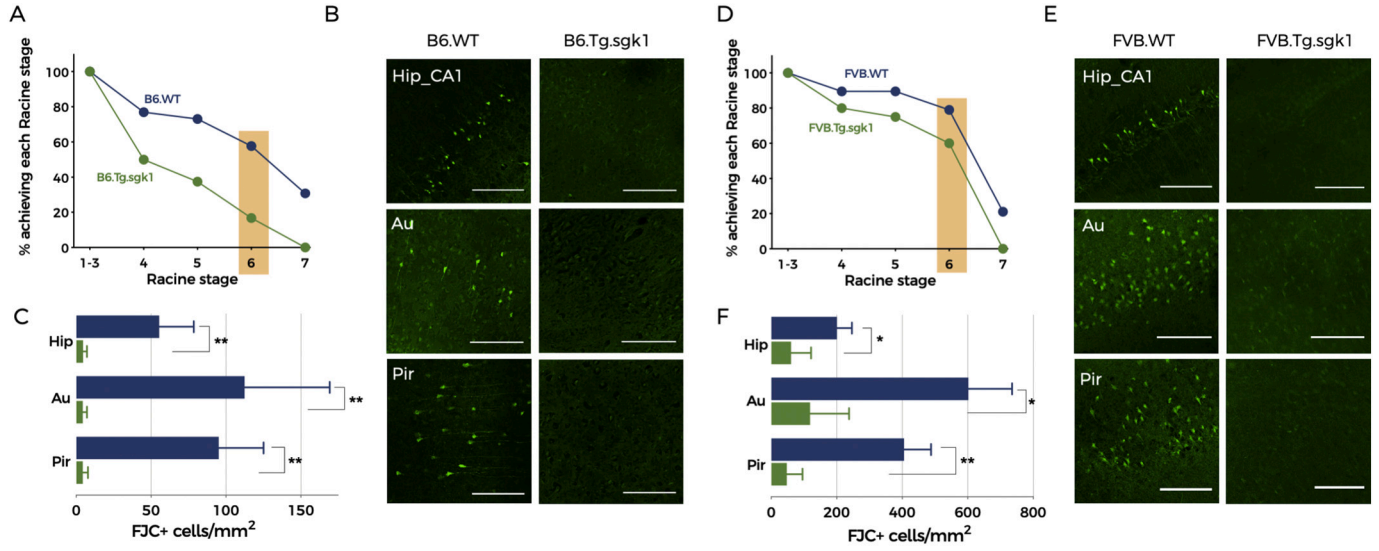

Fig. 1. Fluoro-Jade C staining reveals significantly decreased neuronal death in Tg.sgk1 when compared to WT mice after comparable seizure severity. (A) Cumulative plot representing the percentage of B6.WT (blue) and B6.Tg.sgk1 (green) mice reaching the indicated Racine stages after KA injection. Stage 7 corresponds to death associated to SE. Only mice reaching stage 6 were used to evaluate neuronal death (highlighted in orange) (B6.WT $n = 26$, B6.Tg.sgk1 $n = 24$). Part of the data in this graph have been obtained from (Armas-Capote et al., 2020). (B) Representative confocal images of FJC stained brain sections B6.WT (left column) and B6.Tg.sgk1 mice (right column) reaching Racine stage 6. Region CA1 of hippocampus (Hip_CA1), auditive cortex (Au) and piriform cortex (Pir) brain areas are shown. Scale bar = 100 μm. (C) Quantitative analysis of neurodegeneration events (FJC+ cells) normalized to area (mm^2) corresponding to regions shown in B from B6.WT and B6.Tg.sgk1 mice brain slices. Data are mean ± SEM ($n = 5$; Mann-Whitney test, $^{**}p < 0.01$). (D) Cumulative plot representing the percentage of FVB mice reaching the indicated Racine stages. Only mice reaching stage 6 were used to evaluate neuronal death (highlighted in orange) (FVB.WT $n = 19$; FVB.Tg.sgk1 n = 19). (E) Representative confocal images corresponding to FJC staining of brain slices from same regions as B, from FVB.WT (left column) and FVB.Tg.sgk1 mice (right column) reaching Racine stage 6. Scale bar = 100 μm. (F) Quantification of FJC+ cells normalized to area (mm^2) in both genotypes on the FVB genetic background. Data are mean ± SEM ($n = 7$; Mann-Whitney test, $^{*}p < 0.05$, $^{**}p < 0.01$).

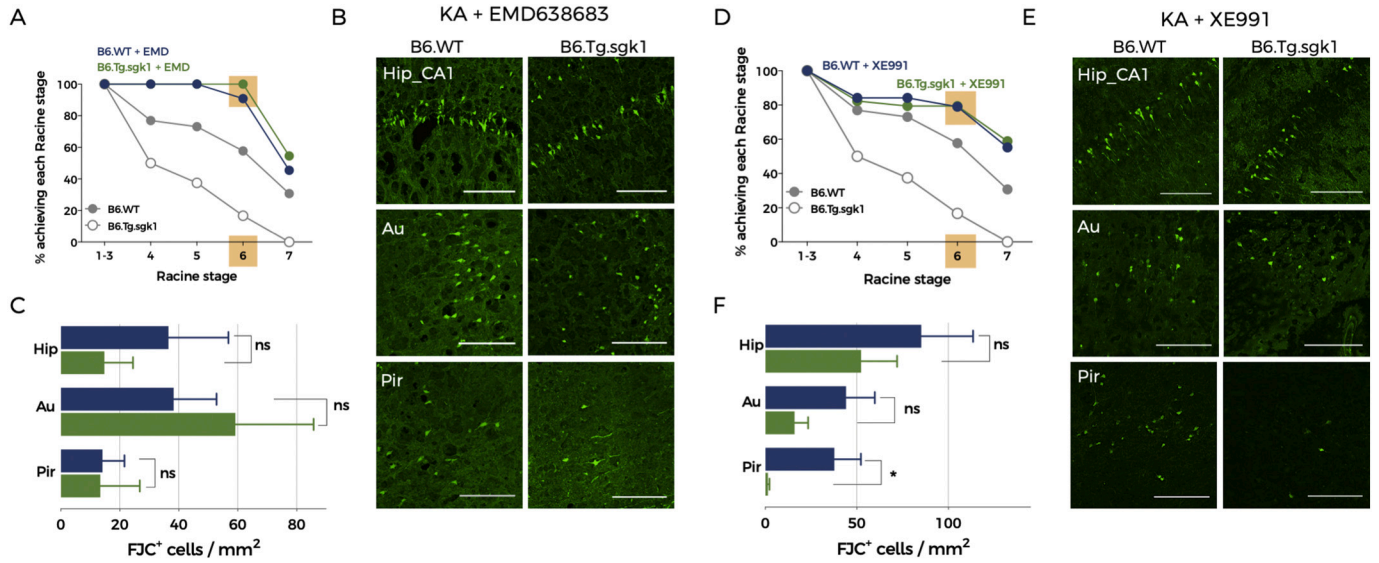

Fig. 2. SGK1.1 activity-dependent neuroprotection includes M-current dependent and independent mechanisms. (A) Cumulative plot representing the percentage of EMD638683-pretreated B6.WT and B6.Tg.sgk1 mice reaching the indicated Racine stages after KA injection. Mice reaching stage 6 were used to evaluate neuronal death (highlighted in orange). Data from EMD638683-untreated animals (Fig. 1A) are shown in grey for reference. (B6.WT n = 26, B6.Tg.sgk1 *n* = 21). (B) Representative confocal images corresponding to FJC staining of brain sections from B6.WT (left column) and B6.Tg.sgk1 mice (right column) pretreated with EMD638683. Brain regions shown are hippocampus (Hip_CA1), auditive cortex (Au) and piriform cortex (Pir). Scale bar = 100 μm. (C) Quantitative analysis of FJC+ cells in EMD638683-pretreated B6.WT (*n* = 8) and B6.Tg.sgk1 (n = 5) mice in the areas shown in B. Data are mean ± SEM (Mann-Whitney test; ns, not significant). (D) Cumulative plot representing the percentage of XE991-pretreated B6.WT and B6.Tg.sgk1 mice reaching the indicated Racine stages after KA injection (B6.WT n = 26, B6.Tg.sgk1 n = 24). Mice reaching stage 6 were used to evaluate neuronal death (highlighted in orange). Data from XE991-untreated animals (Fig. 1A) are shown in grey for reference. Part of the data in this graph have been obtained from (Armas-Capote et al., 2020). (E) Representative images of FJC stained brain sections from animals in D corresponding to hippocampus (Hip_CA1), auditive cortex (Au) and piriform cortex (Pir). Scale bar = 100 μm. (F) Quantitative analysis of FJC+ cells on brain slices from B6.WT and B6.Tg.sgk1 mice in the areas shown in E. Data are mean ± SEM (n = 7; Mann-Whitney test; *$p > 0.05$; ns, not significant).

according to our criteria (*i.e.*, those surviving after reaching Racine stage 6) underwent tonic-clonic seizures for shorter times than WT mice. This was applicable also to transgenic mice treated with the inhibitor (Tg + EMD). As is discussed later, this fact may introduce an apparent inconsistency that prevents us from directly comparing the control groups with and without the inhibitor. Importantly, inactivation of the kinase resulted in identical levels of neuronal death in both genotypes in all brain areas (B6.WT + EMD *vs.* Tg.sgk1 + EMD in Fig. 2B–C). These results demonstrate that kinase activity underlies the mechanism reducing neuronal death associated to KA-induced seizures.

We have previously demonstrated that the regulation of the M-current by SGK1.1 underlies the protection mechanism against seizures progression and severity, since pre-treatment of mice with XE991 fully counteracts the effect of the kinase in transgenic mice (Armas-Capote et al., 2020 and Fig. 2D). Quantification of neuronal death in this experimental condition allowed us to assess the existence of neuroprotective mechanisms that are independent of the alterations in neuronal excitability associated to SGK1.1 activation. Augmented cell excitability in XE991-treated transgenic neurons led to less pronounced differences in neuronal loss between WT and Tg.sgk1 genotypes (Fig. 2D–F). However, we still observed a statistically significant reduction in neuronal death levels at the piriform cortex from Tg.sgk1 mice, and a clear tendency towards decreased death levels in all the other brain areas studied (Fig. 2F). Importantly, piriform, perirhinal and entorhinal cortex have been described as key seizure-trigger zones (Vismer et al., 2015). This result strongly supports the hypothesis that SGK1.1 neuroprotective role may include additional mechanisms that are independent of its effects on neuronal excitability.

3.2. Activation of SGK1.1 reduces levels of reactive gliosis after status epilepticus

Glial cells have an essential role in maintaining brain homeostasis. Growing evidence supports the hypothesis that inflammation is a consequence as well as a cause of epilepsy (for a recent review, see (Patel et al., 2019)). The striking reduction in seizure severity and neuronal death levels associated to SGK1.1 activation led us to hypothesize that other features found in patients with TLE, such as reactive gliosis, would be also reduced in our animal model after the epileptic challenge. To address this question, we quantified the occurrence of gliosis on brain slices from WT and Tg.sgk1 after SE (Racine stage 6). First, GFAP was used as a marker of astrocyte activation to assess astrogliosis levels. As shown in Fig. 3A–B, SGK1.1 activation in Tg.sgk1 mice significantly reduced astrogliosis secondary to KA injection in most brain areas, including hippocampus and cortex. Similar to previous observations, this effect was retained in FVB mice, indicating that it was not associated to specific genetic backgrounds (Fig. 3C–D). Additionally, we measured microgliosis levels using Iba-1 as a marker. Quantitative analysis revealed significantly lower levels of reactive microglia in B6.Tg.sgk1 mice compared to B6.WT (Fig. 4A–B). Similar results were obtained after evaluating the levels of reactive microglia in FVB.WT and FVB.Tg.sgk1 mice, indicating that the effects of SGK1.1 activation on microgliosis are also independent of the genetic background (Fig. 4C–D). Our results unveil a new role of SGK1.1 in diminishing reactivity of glial cells, potentially leading to reduced levels of inflammation and structural changes in the damaged brain.

A potential ramification of the neuroprotective role of SGK1.1 described in the present study could be the existence of deleterious pro-proliferative effects, such as the potential induction of aberrant hippocampal neurogenesis in the DG (Parent et al., 2006). It has been proposed that this ectopic neurogenesis after seizure-induced damage could result in the alteration of neuronal electrophysiological properties, contributing to the generation of hyperexcitable circuits. However, we did not observe significant differences in neuronal proliferation in the granular cell layer (GCL) of Tg.sgk1 *vs.* WT mice (Supplementary Fig. 2). It will be interesting to address in the future whether there is any

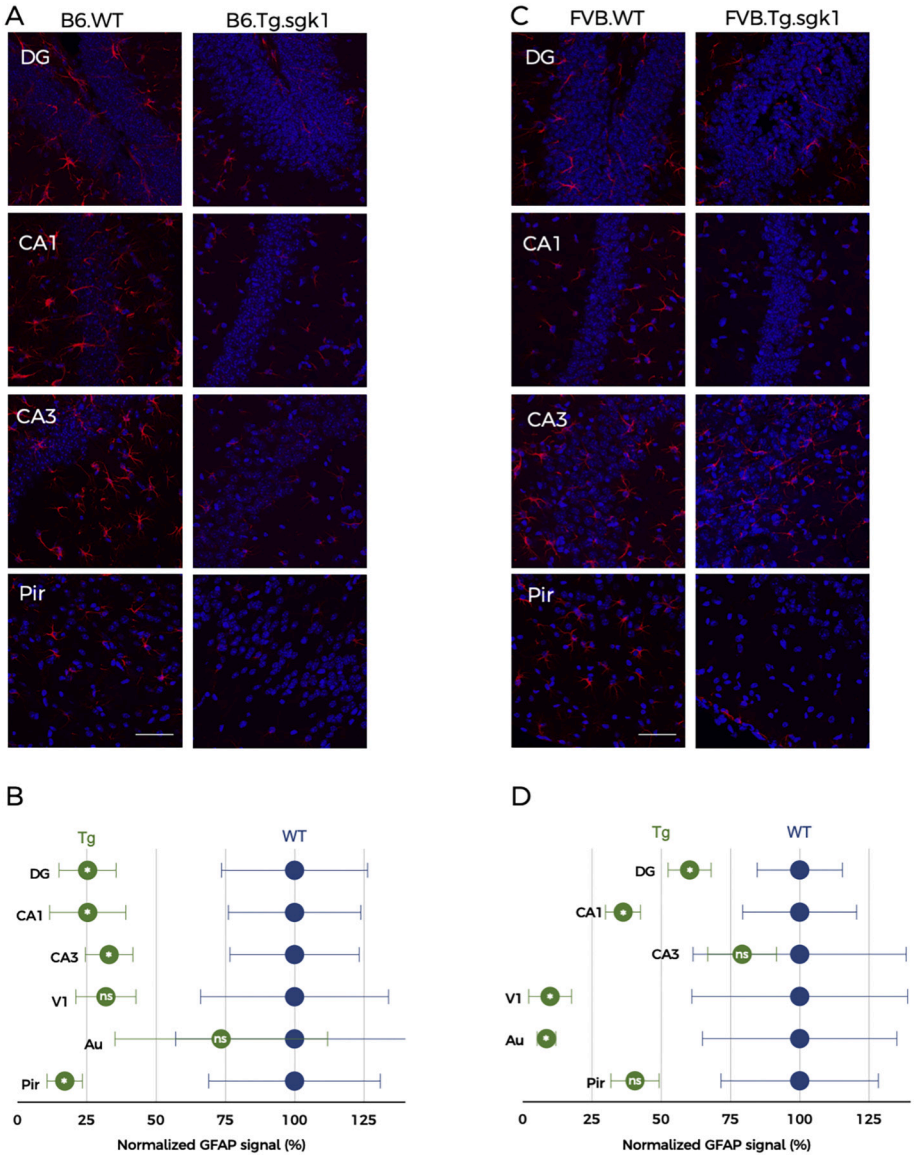

Fig. 3. Astrogliosis is decreased in hippocampus and cortex of KA-injected Tg.sgk1 mice. (A) Representative confocal images showing GFAP immunostaining (red, Alexa 494) and DAPI-stained nuclei (blue) for B6.WT and B6.Tg.sgk1, 72 h after KA injection in hippocampus (regions DG, CA1 and CA3) and piriform cortex (Pir). Scale bar = 50 μm. (B) Average GFAP fluorescent signals measured as 'GFAP area/DAPI area' ratios (see Methods). Data are mean ± SEM, normalized to WT (n = 5; multiple *t*-test; *p < 0,05; ns, not significant). (C) Representative images showing GFAP-positive astrocytes in FVB.WT and FVB.Tg.sgk1 mice, in same regions and experimental conditions as A. (D) Average GFAP fluorescent signals measured as 'GFAP area/DAPI area' ratios (see Methods). Data are mean ± SEM normalized to WT (*n* = 6; multiple t-test; *p < 0,05; **p < 0,01; ns, not significant).

difference in ectopic neurogenesis between Tg.sgk1 and WT mice after KA treatment, both in acute conditions as well as in animals undergoing recurrent spontaneous seizures (acquired epilepsy).

3.3. SGK1.1 is mainly expressed in pyramidal neurons

We next asked whether the effect of constitutively active SGK1.1 on reactive gliosis is directly due to expression of this kinase in glial cells or indirectly related to reduced neuronal death. The distribution of the SGK1.1 protein in the brain has remained elusive, due to the lack of isoform-specific antibodies. To overcome this limitation, we developed a novel rabbit polyclonal antibody raised against an isoform-specific epitope purified from E. coli. The new serum specifically recognized SGK1.1 without cross-reacting with the endogenously expressed ubiquitous isoform SGK1 (Fig. 5A). Thus, HEK cells expressing a control vector containing solely the cyan fluorescent protein (CFP; Fig. 5A, top panels) showed no staining with our SGK1.1 antibody (Alexa 594 channel; Fig. 5A, top middle and right panels). In contrast, clear membrane localization of immunolabelled SGK1.1 in addition to the blue-fluorescent signal from CFP was observed in cells transfected with a fluorescent fusion construct of SGK1.1 (SGK1.1-CFP; Fig. 5A, low middle and right panels). Immunohistochemical localization of SGK1.1 in mouse hippocampus and cortex revealed specific expression in pyramidal neurons as demonstrated by the co-localization with CaMKII (Fig. 5B–C). These results are consistent with our previous report that SGK1.1 mRNA is preferentially expressed in pyramidal neurons of the cortex and hippocampus (Wesch et al., 2010). Interestingly, in hippocampus we observed homogeneous expression in all regions that constitute the glutamatergic circuit involved in excitatory synaptic transmission (see upper panels in Fig. 5B -CA1- and 5E -CA3-). Double immunohistochemistry also revealed that SGK1.1 is not expressed in parvalbumin-positive interneurons (Fig. 5D) or GFAP-expressing astrocytes (Fig. 5E–F), further reinforcing the idea that expression of this kinase is restricted to pyramidal neurons, as previously suggested by *in situ* hybridization (Wesch et al., 2010). Within pyramidal neurons, expression is detectable in the soma and neuronal processes (Fig. 5B and E, left panels), with no positive signal in the nuclei. This localization pattern strongly suggests that SGK1.1 site of action is primarily neuronal and that the decrease in reactive gliosis is secondary to the reduction of neuronal death and not to a direct action of the kinase in glial cells.

3.4. SGK1.1 decreases apoptosis after KA-induced SE

Given the fact that SGK1.1 catalytic domain shares high homology

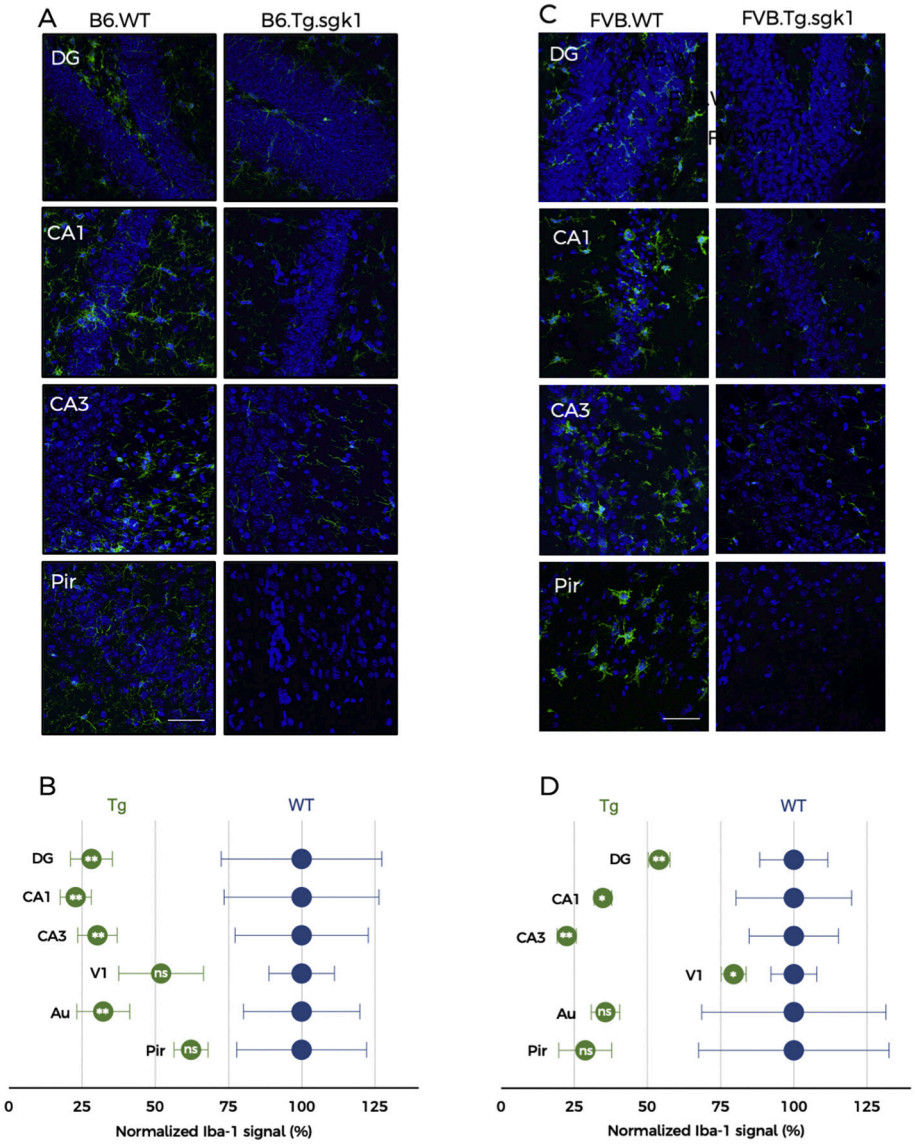

Fig. 4. Microgliosis levels are reduced in Tg.sgk1 *vs.* WT mice after KA treatment. (A) Representative confocal images showing Iba-1 reactivity (green, Alexa 488) and DAPI-stained nuclei (blue) in brain slices from KA-injected B6.WT and B6.Tg.sgk1 mice. Hippocampus regions (DG, CA1 and CA3) and piriform cortex (Pir) are shown. Scale bar = 50 μm. (B) Average Iba-1 levels in transgenic mice compared to WT. Data are mean ± SEM normalized to WT (n = 5; multiple t-test; *p < 0,05; **p < 0.01; ns, not significant). (C) Representative confocal images showing Iba-1 staining in FVB.WT and FVB.Tg.sgk1 brain slices after KA injection in same areas as A. (D) Average Iba-1 levels in transgenic mice compared to WT. Data are mean ± SEM normalized to WT (n = 5; multiple t-test; *p < 0,05; **p < 0.01; ns, not significant).

with the catalytic domain of the well described anti-apoptotic kinase AKT (Kobayashi et al., 1999), and that the ubiquitous isoform SGK1 has anti-apoptotic activity (Ferrelli et al., 2015), we evaluated the ability of SGK1.1 to reduce the levels of apoptosis in an *in vitro* model using the TUNEL assay (Crowley et al., 2016). As previously described, apoptosis levels were significantly reduced in H_2O_2-treated HEK293T cells expressing AKT (Park et al., 2016) (Fig. 6A, middle row and Fig. 6B, grey bar). Heterologous expression of the constitutively active form of SGK1.1 lead to similar results, supporting the potential role of this kinase as an antiapoptotic factor (Fig. 6A-lower row and Fig. 6B, green bar). In contrast, this effect was abolished in cells expressing a kinase-dead mutant of SGK1.1 (K220A) (Fig. 6B, orange bar) (Arteaga et al., 2008; Wesch et al., 2010). Heterologous expression of a mutant with constitutive nuclear localization (FF19.20AA) showed higher sensitivity to H_2O_2-induced apoptosis (Fig. 6B, purple bar), indicating that correct subcellular targeting is essential for SGK1.1 anti-apoptotic effects. Altogether, these results support the idea that SGK1.1 could act as an anti-apoptotic factor *in vivo*, decreasing SE-induced apoptosis in the mouse hippocampus. We tested this hypothesis by quantifying the expression of different markers of apoptotic pathways. First, we evaluated how activation of SGK1.1 in the transgenic mice affected the levels of Bim, a known pro-apoptotic marker of the intrinsic apoptosis pathway (Kim et al., 2014; O'Connor et al., 1998). Western blot analysis performed 24 h after KA-induced SE showed significantly decreased levels of Bim in Tg.sgk1 mice *vs.* WT (Fig. 6C and E). Bands corresponding to the molecular mass of the three existing splice isoforms of Bim (Bim_S, Bim_L and Bim_{EL}) (O'Connor et al., 1998) were detected (Fig. 6C). Additionally, we analyzed the expression of Bcl-x_L, a member of the anti-apoptotic Bcl-2 protein family. This factor has been proposed to reduce apoptosis by preventing mitochondrial permeability transition associated to release of pro-apoptotic factors, therefore contributing to maintain cell viability in the central nervous system (Boise et al., 1993). Consistent with the hypothesis that SGK1.1 activation can exert anti-apoptotic effects, western blot experiments show significantly increased Bcl-x_L protein abundance in the hippocampus of Tg.sgk1 mice *vs.* WT following KA-induced seizures (Fig. 6D and E).

Taken together, our results show that activation of SGK1.1 in pyramidal neurons is a potent mechanism of neuroprotection after SE, with a striking reduction in neuronal death accompanied by a very prominent reduction in reactive gliosis. Mechanistically, this effect underlies a combination of two main factors. In addition to previously demonstrated decreased neuronal excitability due to increased M-current density, we now demonstrate that SGK1.1 activation triggers anti-apoptotic signaling pathways involving altered levels of Bim and Bcl-x_L proteins.

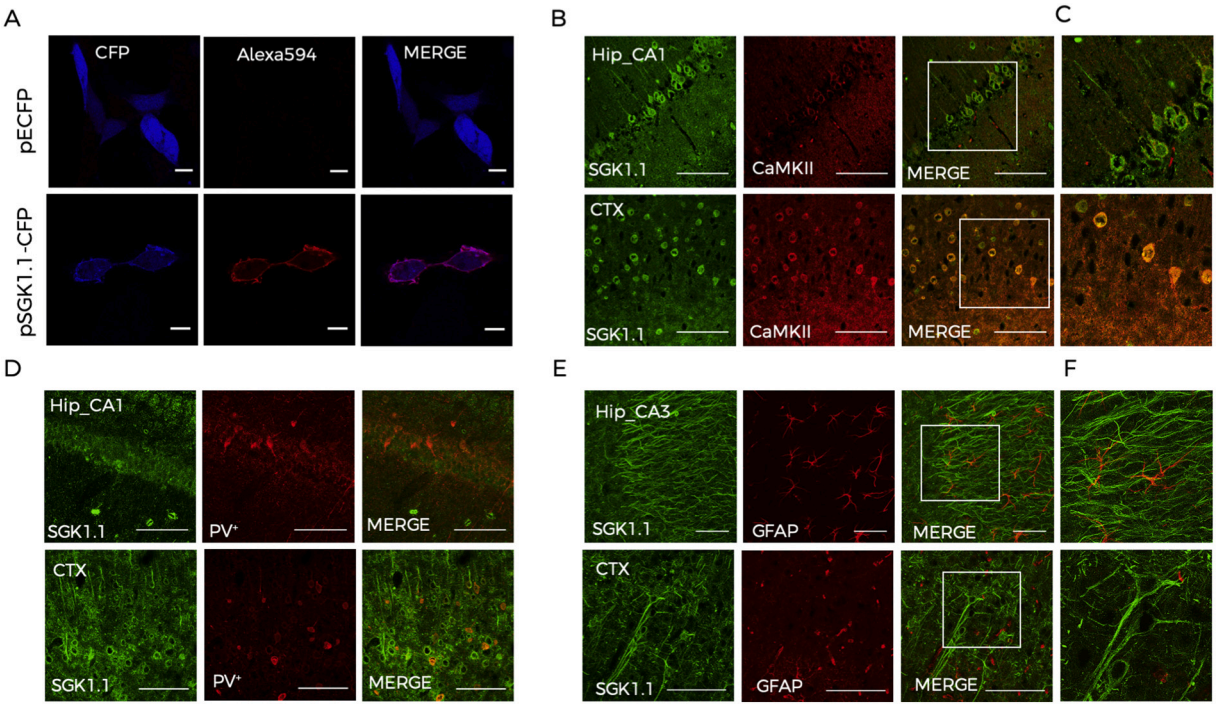

Fig. 5. SGK1.1 is selectively expressed at the soma and processes of pyramidal neurons. (A) Validation of the antibody used in this study. Top panels, representative confocal images of HEK293T cells transfected with a control vector expressing solely the cyan fluorescent protein, CFP (peCFP-N1). Bottom panels, representative images of HEK cells transfected with a fusion construct of SGK1.1 with CFP (SGK1.1-CFP). Images in the left column correspond to the CFP excitation channel (458 nm). The middle column corresponds to immunostaining with our anti-SGK1.1 rabbit polyclonal antibody (Alexa594 excitation channel). Note that red fluorescence corresponding to Alexa594 labelling is specific to cells expressing the SGK1.1 construct. The right column corresponds to the merge of blue and red channels in both conditions. Scale bar = 10 μm. (B) Representative confocal images of WT brain slices showing SGK1.1 (green, Alexa 488) and CaMKII (red, Alexa 594) immunostaining of hippocampus CA1 (Hip_CA1) and visual cortex (CTX) areas. Scale bar = 100 μm. (C) Magnification of white-framed regions in B. (D) Representative confocal images showing SGK1.1 (green) and PV (red) immunostaining of hippocampus CA1 (Hip_CA1) and visual cortex (CTX) from WT brain slices. (E) Representative confocal images showing SGK1.1 (green, Alexa 488) and GFAP (red, Alexa 594) expression of hippocampus CA3 (Hip_CA3) and visual cortex (CTX). (F) Magnification of white-framed areas in E.

4. Discussion

Our work demonstrates that SGK1.1, which has been previously shown as a modulator of Kv7 channels that potently reduces KA-induced seizure severity (Armas-Capote et al., 2020; Miranda et al., 2013), exerts a dual protecting role by additionally modulating and reducing seizure-induced cell damage in the brain. Thus, although SE-induced mortality was increased in wild type mice, we only selected WT and Tg.sgk1 animals surviving after reaching tonic-clonic seizures (Stage 6) for evaluation of brain injury 72 h post-KA. Importantly, the protective effect mediated by SGK1.1 is robust and independent of the genetic background. It is maintained in FVB/NJ mice, a strain associated to higher levels of neurodegeneration than C57BL/6 J (Loscher et al., 2017). Neuroprotection is due to SGK1.1 activation, since acute kinase inhibition with the specific inhibitor EMD638683 lead to equal levels of neuronal death in both genotypes. This result also rules out that the observed effects are a consequence of long-term changes induced by the expression of the transgene. Regarding these experiments, it is important to note an apparent inconsistency when comparing the amount of cell death between controls in Figs. 1C and 2C. As mentioned above, treatment with EMD led to higher rates of mortality in both genotypes (Fig. 2A) and, as a consequence, we were only able to include animals surviving Racine stage 6 for shorter times than B6.WT and B6.Tg.sgk1. Therefore, it is not possible to directly compare Fig. 1C with Fig. 2C. However, we would argue that the comparison most relevant in this study is that of WT and transgenic mice both treated with EMD638683. Our results show that inactivation of the kinase completely abrogates the protective effect: the levels of neuronal death are indistinguishable between genotypes after treatment with the kinase inhibitor. Inhibition of the M-current by pre-treatment with the Kv7 blocker XE991 abolished differences in behavioral seizures between genotypes (Fig. 2), as well as the decrease in CA1 excitability associated to activation of the kinase (Armas-Capote et al., 2020). Strikingly, transgenic mice still showed significantly reduced neuronal death levels in relevant brain areas after the KA challenge, suggesting that activation of SGK1.1 modulates pathways preventing neuronal death independently of its role in membrane Kv7 modulation.

The mechanism underlying this observed SGK1.1-mediated protection against neuronal death relies at least partially on the role of this kinase as an anti-apoptotic factor in the brain. First, our data show that SGK1.1 activation reduces H_2O_2-induced apoptosis to similar extents than AKT. This finding is not surprising, given the shared homology of SGK1.1 and AKT catalytic domains. Further, the existence of such homology makes it tempting to hypothesize that both kinases might share downstream substrates including the anti-apoptotic transcriptional factor Bim, which has been related to SE-brain damage with FOXO3a and caspase-3 (Kim et al., 2014). Consistent with this notion, we now show that activation of SGK1.1 in Tg.sgk1 mice reduces Bim protein levels in hippocampus, whereas Bcl-x_L is upregulated. Importantly, both members of the Bcl-2 family have been described as key regulators of the mitochondrial (intrinsic) apoptotic pathway (Youle and Strasser, 2008) and related to seizure-induced brain damage (Kim et al., 2014; Murphy et al., 2010). Increased levels of Bim have been reported in mice and rats after KA-induced SE, while Bim-deficient mice show reduced levels of neurodegeneration (Bouillet et al., 1999; Murphy et al., 2010). Bim localizes to intracellular membranes, where it has been proposed to induce apoptotic cell death *via* caspase activation (O'Connor et al., 1998). This proapoptotic effect is blocked by interaction with Bcl-xL, an anti-

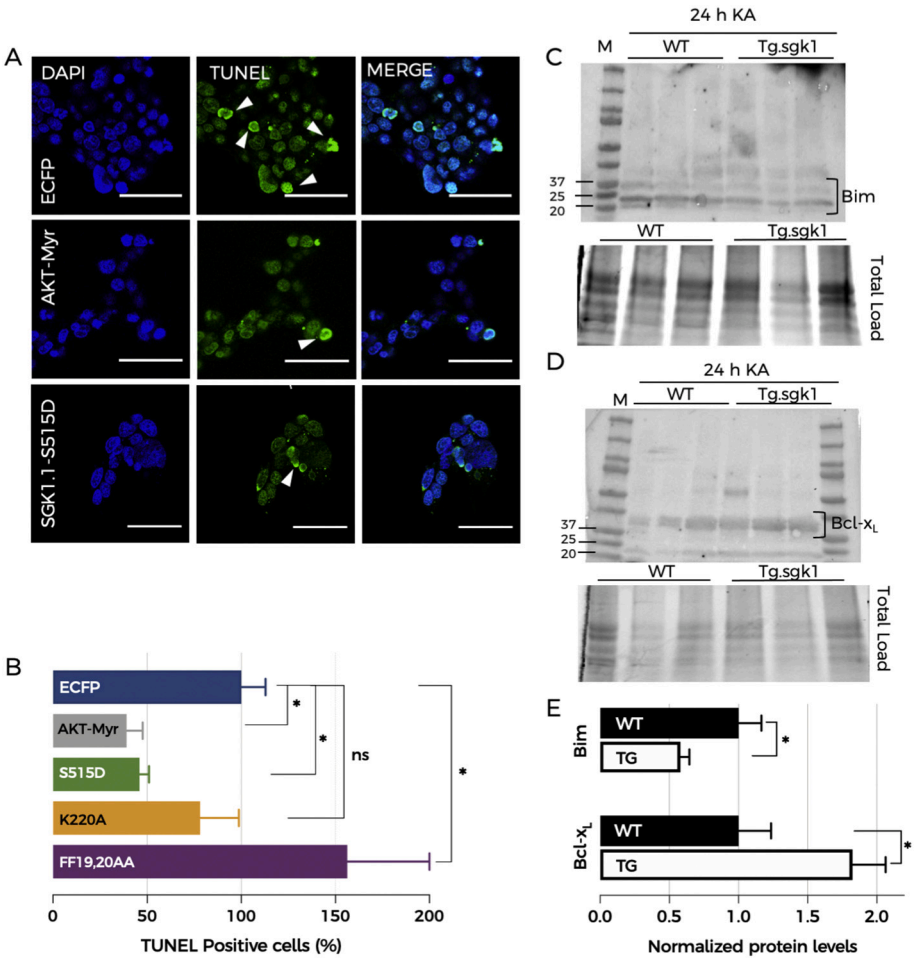

Fig. 6. SGK1.1 activation exerts anti-apoptotic effects *via* modulation of apoptosis mediators after KA-induced SE. (A) Representative confocal images of cells transfected with the indicated constructs. Arrows point to TUNEL-positive cells (fluorescein-stained). Blue fluorescence corresponds to DAPI staining. Scale bar = 10 μm. (B) Quantitative analysis of TUNEL-positive cells proportion (corrected by the total number of cells quantified with DAPI) after transfection with the indicated constructs and H_2O_2 treatment. Bars show mean ± SEM. Values are normalized to those of cells expressing the pECFP-N1 control (n = 5; one-way ANOVA followed by multiple comparison test; * $p < 0.05$; ns, not significant). (C) *Top*, Representative western blot of Bim protein abundance in the hippocampus of WT and transgenic mice 24 h after KA administration. *Bottom*, total protein loading. (D) *Top*, Representative western blot of Bcl-x_L protein abundance in the hippocampus of WT and transgenic mice 24 h after KA administration. *Bottom*, total protein loading. (E) Quantification of western blot data. Bars represent mean ± SEM from WT ($n = 4$) and Tg.sgk1 (n = 6; Unpaired t-test; *$p < 0.05$).

apoptotic factor found in mature neurons in the adult brain. Accordingly, Bcl-x_L-deficient mice show massive neuronal cell death (Motoyama et al., 1995). Our results showing modulation of both factors in transgenic mice are consistent with the observed significantly lower levels of neurodegeneration that are associated to activation of SGK1.1. Importantly, it has been described that upon activation of AMPA and KA receptors by KA, increases in intracellular Ca^{2+} and generation of ROS rapidly lead to damage of intracellular membranes and activation of apoptotic pathways responsible for neuronal death. Alternatively, necrosis might be also occurring as a result of Ca^{2+} overload (Wang et al., 2005).

Neurodegeneration has been described as one of the most common alterations found in epilepsy patients contributing to progression towards a sclerotic and hardened brain (Goldberg and Coulter, 2013; Mathern et al., 1997). Although there is a growing body of evidence supporting that neuroprotection does not prevent development of acquired epilepsy (André et al., 2001; Brandt et al., 2003; Pitkänen, 2002), it has been proven that alleviation of neurodegeneration diminishes adverse effects of SE and might improve recovery (Pitkänen and Kubova, 2004). Proinflammatory mediators, reactive astrocytes and microglia have been found in the resected hippocampi of TLE patients and might contribute to the generation of new seizures (Aronica et al., 2007; Ravizza et al., 2008). However, it is not clear whether inflammation is a consequence or a cause of epilepsy (Vezzani et al., 2011). In the present work, we demonstrate that while SGK1.1 is not expressed in astrocytes, its neuronal activation prevents reactive gliosis in a transgenic mouse model, limiting the extent of overall brain damage. It is important to note that this decrease in gliosis could be secondary to the decrease in neuronal death and does not reflect a new role of SGK1.1 in glial cells.

Although epilepsy research has allowed the development and improvement of different available treatments, there is still a great need for approaches able to control seizures in approximately 30% of the patients showing resistance to antiepileptic drugs (Löscher and Schmidt, 2011). New strategies suitable to diminish and reduce brain damage after SE might help to prevent the progression of the disease as well as the deterioration of neuronal tissue, which is usually accompanied by a long list of comorbidities and psychiatric dysfunctions (Elliott et al., 2009; Kanner et al., 2010; Tellez-Zenteno et al., 2007). The present work, together with our previously published results (Armas-Capote et al., 2020; Miranda et al., 2013) strongly supports a dual role of SGK1.1 as an anti-convulsant and neuroprotective factor. It will be interesting to establish if the effects observed here in acute conditions are extrapolated to animal models of acquired epilepsy, which could open new therapeutic avenues in this disease.

Funding

This work was supported by the Ministerio de Economia y Competitividad-MINECO, Spain [grant numbers BFU2015-66490-R, RTI2018-098768-B-I00, BFU2015-70067-REDC, and a F.P.I. predoctoral Fellowship (BES-2016-077337) to E.M.B.]; the European Research Council (ERC) under the European Union''s Horizon 2020 research and innovation programme [grant agreement 648936].

CRediT authorship contribution statement

Elva Martin-Batista: conceptualization, investigation, formal analysis, writing-original draft, writing-review & editing, visualization.

Laura E. Maglio: conceptualization, investigation, formal analysis, writing original draft, writing-review & editing, visualization. **Natalia Armas-Capote:** investigation, formal analysis. **Guadalberto Hernández:** investigation, validation. **Diego Alvarez de la Rosa:** conceptualization, formal analysis, writing-original draft, writing-review & editing, visualization. **Teresa Giraldez:** conceptualization, formal analysis, writing-original draft, writing-review & editing, funding acquisition, supervision, visualization, project administration, validation.

Acknowledgments

We thank Dr. Tomás Gonzalez and Dr. Pedro Barroso for the help with FJC protocol.

Appendix A. Supplementary data

Supplementary data to this article can be found online at https://doi.org/10.1016/j.nbd.2021.105317.

References

Ackermann, T.F., et al., 2011. EMD638683 , a novel SGK inhibitor with antihyper- tensive potency. Cell. Physiol. Biochem. 137–146.
Afonso-Oramas, D., et al., 2010. The dopamine transporter is differentially regulated after dopaminergic lesion. Neurobiol. Dis. 40, 518–530.
André, V., et al., 2001. Vigabatrin protects against hippocampal damage but is not antiepileptogenic in the lithium-pilocarpine model of temporal lobe epilepsy. Epilepsy Res. 47, 99–117.
Armas-Capote, N., 2017. The Serum and Glucocorticoids Regulated Kianse 1.1 (SGK1.1) as an Anticonvulsant Factor.
Armas-Capote, N., et al., 2020. SGK1.1 reduces Kainic acid-induced seizure severity and leads to rapid termination of seizures. Cereb. Cortex 30, 3184–3197.
Aronica, E., et al., 2007. Complement activation in experimental and human temporal lobe epilepsy. Neurobiol. Dis. 26, 497–511.
Arteaga, M.F., et al., 2008. A brain-speciffc SGK1 splice isoform regulates expression of ASIC1 in neurons. Proc. Natl. Acad. Sci. U. S. A. 105, 4459–4464.
Ben-Ari, Y., et al., 1979. A new model of focal status epilepticus: intra-amygdaloid application of kainic acid elicits repetitive secondarily generalized convulsive seizures. Brain Res. 163, 176–179.
Benkovic, S.A., et al., 2004. Sensitive indicators of injury reveal hippocampal damage in C57BL/6J mice treated with kainic acid in the absence of tonic-clonic seizures. Brain Res. 1024, 59–76.
Boise, L.H., et al., 1993. Bcl-X, a Bcl-2-related gene that functions as a dominant regulator of apoptotic cell death. Cell. 74, 597–608.
Bouillet, P., et al., 1999. Proapoptotic Bcl-2 relative Bim required for certain apoptotic responses, leukocyte homeostasis, and to preclude autoimmunity. Science. 286, 1735–1738.
Brandt, C., et al., 2003. N-methyl-D-aspartate receptor blockade after status epilepticus protects against limbic brain damage but not against epilepsy in the kainate model of temporal lobe epilepsy. Neuroscience. 118, 727–740.
Brunet, A., et al., 2001. Protein kinase SGK mediates survival signals by phosphorylating the Forkhead transcription factor FKHRL1 (FOXO3a). Mol. Cell. Biol. 21, 952–965.
Coric, T., et al., 2004. Expression of ENaC and serum- and glucocorticoid-induced kinase 1 in the rat intestinal epithelium. Am. J. Physiol. Gastrointest. Liver Physiol. 286.
Crowder, R.J., Freeman, R.S., 1998. Phosphatidylinositol 3-kinase and Akt protein kinase are necessary and sufffcient for the survival of nerve growth factor-dependent sympathetic neurons. J. Neurosci. 18, 2933–2943.
Crowley, L.C., et al., 2016. Detection of DNA fragmentation in apoptotic cells by TUNEL. Cold Spring Harb Protoc 2016.
Datta, S.R., et al., 1997. Akt phosphorylation of BAD couples survival signals to the cell-intrinsic death machinery. Cell. 91, 231–241.
Elliott, J.O., et al., 2009. Comorbidity, health screening, and quality of life among persons with a history of epilepsy. Epilepsy Behav. 14, 125–129.
Ferrelli, F., et al., 2015. Serum glucocorticoid inducible kinase (SGK)-1 protects endothelial cells against oxidative stress and apoptosis induced by hyperglycaemia. Acta Diabetol. 52, 55–64.
Frangioni, J.V., Neel, B.G., 1993. Solubilization and puriffcation of enzymatically active glutathione S-transferase (pGEX) fusion proteins. Anal. Biochem. 210, 179–187.
Franklin, K., Paxinos, G., 2008. The Mouse Brain in Stereotaxic Coordinates. Academic Press, Elsevier.
Goldberg, E.M., Coulter, D.A., 2013. Mechanisms of epileptogenesis: a convergence on neural circuit dysfunction. Nat. Rev. Neurosci. 14, 337–349.
Henshall, D.C., et al., 2002. Activation of Bcl-2-associated death protein and counterresponse of Akt within cell populations during seizure-induced neuronal death. J. Neurosci. 22, 8458–8465.
Hopkins, K.J., et al., 2000. Temporal progression of kainic acid induced neuronal and myelin degeneration in the rat forebrain. Brain Res. 864, 69–80.
Kanner, A.M., et al., 2010. Postictal affective episodes. Epilepsy Behav. 19, 156–158.
Kim, Y.S., et al., 2014. Decreased interaction between FoxO3a and Akt correlates with seizure-induced neuronal death. Epilepsy Res. 108, 367–378.
Klement, W., et al., 2018. Seizure progression and infiammatory mediators promote pericytosis and pericyte-microglia clustering at the cerebrovasculature. Neurobiol. Dis. 113, 70–81.
Kobayashi, T., Cohen, P., 1999. Activation of serum- and glucocorticoid-regulated protein kinase by agonists that activate phosphatidylinositide 3-kinase is mediated by 3-phosphoinositide-dependent protein kinase-1 (PDK1) and PDK2. Biochem. J. 339 (Pt 2), 319–328.
Kobayashi, T., et al., 1999. Characterization of the structure and regulation of two novel isoforms of serum- and glucocorticoid-induced protein kinase. Biochem. J. 344 (Pt 1), 189–197.
Levesque, M., et al., 2016. Animal models of temporal lobe epilepsy following systemic chemoconvulsant administration. J. Neurosci. Methods 260, 45–52.
Löscher, W., Schmidt, D., 2011. Modern antiepileptic drug development has failed to deliver: ways out of the current dilemma. Epilepsia. 52, 657–678.
Loscher, W., et al., 2017. The relevance of inter- and intrastrain differences in mice and rats and their implications for models of seizures and epilepsy. Epilepsy Behav. 73, 214–235.
Mathern, G.W., et al., 1997. Hippocampal sclerosis. In: Epilepsy: A Comprehensive Textbook, pp. 133–155.
McCaig, C.A.P., Shtaya, A., Omar, A.S., Green, A.R., Kind, C.N., Pereira, A.C., Naray-Fejes-Toth, A., Fejes-Toth, G., Yáñez-Muñoz, R.J., Murray, J.T., Jainsworth, A.H., 2019. Induction of cell survival kinase Sgk1: a possible novel mechanism for α-phenyl-N-tert-butylnitrone in experimental stroke. J. Cereb. Blood Flow Metab. 39, 1111–1121.
Miranda, P., et al., 2013. The neuronal serum- and glucocorticoid-regulated kinase 1.1 reduces neuronal excitability and protects against seizures through upregulation of the M-current. J. Neurosci. 33, 2684–2696.
Motoyama, N., et al., 1995. Massive cell death of immature hematopoietic cells and neurons in Bcl-x-deffcient mice. Science. 267, 1506–1510.
Murphy, B.M., et al., 2010. Contrasting patterns of Bim induction and neuroprotection in Bim-deffcient mice between hippocampus and neocortex after status epilepticus. Cell Death Differ. 17, 459–468.
O'Connor, L., et al., 1998. Bim: a novel member of the Bcl-2 family that promotes apoptosis. EMBO J. 17, 384–395.
Parent, J.M., et al., 2006. Aberrant seizure-induced neurogenesis in experimental temporal lobe epilepsy. Ann. Neurol. 59, 81–91.
Park, J.H., et al., 2016. Akt attenuates apoptotic death through phosphorylation of H2A under hydrogen peroxide-induced oxidative stress in PC12 cells and hippocampal neurons. Sci. Rep. 6, 21857.
Patel, D.C., et al., 2019. Neuron–glia interactions in the pathophysiology of epilepsy. Nat. Rev. Neurosci. 20, 282–297.
Pitkänen, A., 2002. Efffcacy of current antiepileptics to prevent neurodegeneration in epilepsy models. Epilepsy Res. 50, 141–160.
Pitkänen, A., Kubova, H., 2004. Antiepileptic drugs in neuroprotection. Expert. Opin. Pharmacother. 5, 777–798.
Pitkanen, A., Lukasiuk, K., 2009a. Epilepsy: neuronal death. In: Encyclopedia of Neuroscience. Academic Press.
Pitkanen, A., Lukasiuk, K., 2009b. Molecular and cellular basis of epileptogenesis in symptomatic epilepsy. Epilepsy Behav. 14 (Suppl. 1), 16–25.
Ramaswamy, S., et al., 1999. Regulation of G1 progression by the PTEN tumor suppressor protein is linked to inhibition of the phosphatidylinositol 3-kinase/Akt pathway. Proc. Natl. Acad. Sci. U. S. A. 96, 2110–2115.
Ravizza, T., et al., 2008. Innate and adaptive immunity during epileptogenesis and spontaneous seizures: evidence from experimental models and human temporal lobe epilepsy. Neurobiol. Dis. 29, 142–160.
Roy, M., et al., 2002. HSV-mediated delivery of virally derived anti-apoptotic genes protects the rat hippocampus from damage following excitotoxicity, but not metabolic discruption. Gene Ther. 9, 214–219.
Schindelin, J., et al., 2012. Fiji: an open-source platform for biological-image analysis. Nat. Methods 9, 676–682.
Schmued, L.C., et al., 2005. Fluoro-jade C results in ultra high resolution and contrast labeling of degenerating neurons. Brain Res. 1035, 24–31.
Sharma, A.K., et al., 2007. Mesial temporal lobe epilepsy: pathogenesis, induced rodent models and lesions. Toxicol. Pathol. 35, 984–999.
Sharma, S., et al., 2018. Status Epilepticus: behavioral and electroencephalography seizure correlates in Kainate experimental models. Front. Neurol. 9, 7.
Takahashi, D.K., et al., 2010. Increased coupling and altered glutamate transport currents in astrocytes following kainic-acid-induced status epilepticus. Neurobiol. Dis. 40, 573–585.
Tellez-Zenteno, J.F., et al., 2007. Psychiatric comorbidity in epilepsy: a population-based analysis. Epilepsia. 48, 2336–2344.
Trinka, E., et al., 2015. A deffnition and classiffcation of status epilepticus - report of the ILAE task force on classiffcation of status Epilepticus. Epilepsia. 56, 1515–1523.
Vezzani, A., et al., 2011. The role of infiammation in epilepsy. Nat. Rev. Neurol. 7, 31–40.
Vismer, M.S., et al., 2015. The piriform, perirhinal, and entorhinal cortex in seizure generation. Front. Neural Circ. 9, 1–14.
Wang, Q., et al., 2005. Kainic acid-mediated excitotoxicity as a model for neurodegeneration. Mol. Neurobiol. 31, 3–16.
Wang, D.H.Z., Li, L., Yuan, Y., Xiang, L., Ni, C., Yu, W., 2019. Intracarotid cold saline infusion contributes to neuroprotection in MCAO-induced ischemic stroke in rats via serum and glucocorticoid-regulated kinase 1. Mol. Med. Rep. 20, 3942–3950.
Wesch, D., et al., 2010. The neuronal-speciffc SGK1.1 kinase regulates –delta"-epithelial Na+ channel independently of PY motifs and couples it to phospholipase C signaling. Am. J. Phys. Cell Phys. 299, C779–C790.
Yan, B.C., et al., 2018. Changes in the blood-brain barrier function are associated with hippocampal neuron death in a Kainic acid mouse model of epilepsy. Front. Neurol. 9, 775.
Yang, X.W., Gong, S., 2005. An overview on the generation of BAC transgenic mice for neuroscience research. In: Curr Protoc Neurosci. Chapter 5, Unit 5 20.

Youle, R.J., Strasser, A., 2008. The BCL-2 protein family: opposing activities that mediate cell death. Nat. Rev. Mol. Cell Biol. 9, 47–59.
Zaczek, R., et al., 1998. Two new potent neurotransmitter release enhancers, 10,10-bis(4-pyridinylmethyl)-9(10H)-anthracenone and 10,10-bis(2-fiuoro-4-pyridinylmethyl)-9(10H)-anthracenone: comparison to linopirdine. J. Pharmacol. Exp. Ther. 285, 724–730.
Zanuzzi, C.N., et al., 2019. Reactivity of microglia and astrocytes after an excitotoxic injury induced by kainic acid in the rat spinal cord. Tissue Cell 56, 31–40.